RSC Advances

PAPER

View Article Online
View Journal | View Issue

Cite this: *RSC Adv.*, 2023, **13**, 12153

Janus structures of the C_{2h} polymorph of gallium monochalcogenides: first-principles examination of Ga_2XY (X/Y = S, Se, Te) monolayers

Tuan-Anh Tran, [a] Le S. Hai,[a] Vo T. T. Vi, [b] Cuong Q. Nguyen, [cd] Nguyen T. Nghiem,[e] Le T. P. Thao[f] and Nguyen N. Hieu *[cd]

Group III monochalcogenide compounds can exist in different polymorphs, including the conventional D_{3h} and C_{2h} phases. Since the bulk form of the C_{2h}-group III monochalcogenides has been successfully synthesized [*Phys. Rev. B: Condens. Matter Mater. Phys.* **73** (2006) 235202], prospects for research on their corresponding monolayers have also been opened. In this study, we design and systematically consider a series of Janus structures formed from the two-dimensional C_{2h} phase of gallium monochalcogenide Ga_2XY (X/Y = S, Se, Te) using first-principles simulations. It is demonstrated that the Janus Ga_2XY monolayers are structurally stable and energetically favorable. Ga_2XY monolayers exhibit high anisotropic mechanical features due to their anisotropic lattice structure. All Janus Ga_2XY are indirect semiconductors with energy gap values in the range from 1.93 to 2.67 eV. Due to the asymmetrical structure, we can observe distinct vacuum level differences between the two surfaces of the examined Janus structures. Ga_2XY monolayers have high electron mobility and their carrier mobilities are also highly directionally anisotropic. It is worth noting that the Ga_2SSe monolayer possesses superior electron mobility, up to 3.22×10^3 cm^2 V^{-1} s^{-1}, making it an excellent candidate for potential applications in nanoelectronics and nanooptoelectronics.

Received 16th February 2023
Accepted 13th April 2023

DOI: 10.1039/d3ra01079a

rsc.li/rsc-advances

1 Introduction

For nearly two decades, the field of materials science has grown and expanded dramatically. Particularly, the family of two-dimensional (2D) nanomaterials has received extensive attention and research from the scientific community, both theoretically and experimentally. Emerging in the family of two-dimensional materials is a class of group III monochalcogenides MX, which have been experimentally fabricated, such as InSe,[1] GaS,[2] and GaSe.[3] Physical properties of group III monochalcogenide compounds MX (M = Ga, In; X = S, Se, Te) have been systematically studied recently.[4–6] It has been shown that this class of materials has outstanding physical properties and diverse applications in the fields of nanooptoelectronics such as nanophotodetectors, field-effect transistors and so on.

Recently, the vertical asymmetric structure, namely the Janus structure of 2D nanomaterials, have been experimentally fabricated.[7,8] As a result, a series of new Janus structures have been designed and studied extensively.[9–12] Notable for this continuum is the Janus configurations based on group III monochalcogenide monolayers.[13–15] The Janus group III monochalcogenide compounds M_2XY were predicted to be dynamically and thermodynamically stable.[16] The M_2STe and M_2SeTe monolayers are direct bandgap semiconductors,[17–19] while the MXs are indirect bandgap ones. It can be realized that the electronic band structure is changed when the structural symmetry of the material is broken. Besides, the oxygenation of Janus monochalcogenides has also been reported in many previous works.[9,14,20] These oxidized monolayers were shown to exhibit stability, and the oxygenation caused the semiconductor-to-metal phase transitions in OGaInSe and OGaInTe structures.[9] The high electron mobility in GaInXO system makes this Janus potentially applicable in nanoelectronic devices.

It is well-known that the 2D structures can exist in various polymorphs.[21,22] The discovery of different crystal phases of material has provided novel characteristics and applications. MoS_2 monolayer can exist in the 2H phase as well as in the 1T′ phase.[23,24] Also, group III monochalcogenide InSe monolayer can be stable in both D_{3d} phase[25] and D_{3h} phase.[26] Not only that, the InSe bulk belonging to the C_{2h} point group has been

[a]*Faculty of Applied Sciences, Ho Chi Minh City University of Technology and Education, Ho Chi Minh City, Vietnam*
[b]*Faculty of Basic Sciences, University of Medicine and Pharmacy, Hue University, Hue, Vietnam*
[c]*Institute of Research and Development, Duy Tan University, Da Nang, Vietnam. E-mail: nguyenngochieu1@dtu.edu.vn*
[d]*Faculty of Natural Sciences, Duy Tan University, Da Nang, Vietnam*
[e]*Graduate University of Science and Technology, Vietnam Academy of Science and Technology, Ha Noi, Vietnam*
[f]*Faculty of Physics, University of Science and Education, The University of Da Nang, Da Nang, Vietnam*

successfully fabricated experimentally.[27,28] This discovery prompted scientists to hope for the possibility of synthesizing the corresponding C_{2h} phase of 2D group III monochalcogenide materials. Theoretical studies have predicted the stability of C_{2h} group III monochalcogenide monolayers.[29] MX materials with C_{2h} space group are semiconductors with wider direct bandgaps and their carrier mobilities are much higher than that in the conventional D_{3h} phase. C_{2h}-MX has a strong absorption coefficient and anisotropic optical properties, making new phase potential for application in high-performance optoelectronic devices.[29]

Following this development, we propose a series of Janus Ga_2XY monolayers based on C_{2h}-GaX materials by means of density functional theory. We first focus on their structural features and stability. Besides, the electronic characteristics and also carrier mobilities of Ga_2XY are calculated systematically. The article is structured as follows. The next section presents the methodology and computational methods used in this study. The main calculated results of the paper are presented in Section III, including crystal structure characteristics and structural stability, electronic properties, and carrier mobility. The conclusion is presented in Section IV.

2 Computational method

All calculations in this study were computed based on density functional theory (DFT) performed by Quantum Espresso code.[30] We used the projector augmented wave approximation to investigate the electron–ion interaction.[31] The cut-off energy of 50 Ry was selected for a plane-wave basis. The electron exchange and correlation effect were considered by the functional suggested by Perdew, Burke, and Ernzerhof (PBE).[32] Further, we also used Heyd–Scuseria–Ernzerhof (HSE06) hybrid functional[33] as implemented in the Vienna *ab initio* simulation code[34,35] to correct bandgap of the investigated structures. A *k*-points grid of $(15 \times 15 \times 1)$ was chosen for sampling the first Brillouin zone by the Monkhorst–Pack scheme.[36] The convergence threshold of energy and force was selected as 10^{-6} eV and 10^{-3} eV Å^{-1}, respectively. The weak van der Waals forces between interlayers were treated by the semiempirical DFT-D3 method[37] was adopted to describe the weak van der Waals (vdW) interactions between interlayers. A vacuum space of 20 Å was used along the vertical direction to eliminate possible interactions between neighbor slabs. The phonon dispersions were calculated by the density functional perturbation approximation[38] as implemented in the PHONOPY software.[39] To test the thermodynamic stability of Janus systems, the *ab initio* molecular dynamics (AIMD) calculation was performed.[40] The carrier mobilities in these Janus were determined based on the deformation potential (DP) theory.[41]

3 Results and discussion

3.1 Crystal structure and structural stabilities

Fig. 1 presents the optimized crystal structure of Janus Ga_2XY monolayer, which is a monoclinic lamella. The Janus Ga_2XY, as shown in Fig. 1, can be formed by substituting the top

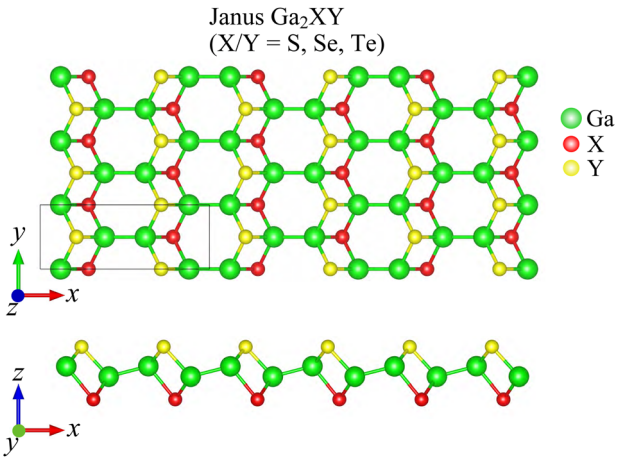

Fig. 1 Top and side views of crystal structure of Janus Ga_2XY structure (X/Y = S, Se, Te).

chalcogen atom layer X with another chalcogen atom layer Y in the C_{2h}-GaX monolayer. The unit cell of Ga_2XY contains eight atoms and its crystal structure belongs to the symmetry group *Pm* (C_s). This is different from the C_{3v}-Ga_2XY monolayer (formed from D_{3h}-GaX), where the unit cell contains only four atoms.[42] The structural parameters for optimized crystals of Ga_2XY monolayers are presented in Table 1. We can see that Janus Ga_2XY is a high anisotropic structure with the anisotropic ratio $\tau = a/b$ (a and b are the lattice constants) up to about 2.6. The lattice constants increase with the increasing atomic size of the chalcogen atoms X and Y. The lattice constant value a/b ranges from 9.77/3.70 Å (Ga_2SSe) to 9.90/3.94 Å (Ga_2SeTe). It is demonstrated that the lattice parameter b of Ga_2SSe is between that of GaS and GaSe,[29] while the lattice constant a of Ga_2SSe is smaller than that of both GaS and GaSe.

We next test the structural stabilities of the investigated materials. Firstly, we evaluate the strength of the chemical bonding between atoms in Janus Ga_2XY monolayers through the calculations for cohesive energy E_{coh} by the following:

$$E_{coh} = \frac{E_{tot} - (N_{Ga}E_{Ga} + N_X E_X + N_Y E_Y)}{N_{Ga} + N_X + N_Y}, \quad (1)$$

Here E_{tot} is the total energy of Janus material; E_{Ga}, E_X, and E_Y are the energies of individual elements Ga, X, and Y, respectively; N_{Ga}, N_X, and N_Y are the number of Ga, X and Y atoms in unit cell, respectively.

In Table 1, we present the calculated values of the cohesive energies of the Ga_2XY monolayers. The cohesive energies of Ga_2SSe, Ga_2STe and Ga_2SeTe are calculated to be −4.01, −3.79 and −3.63 eV per atom, respectively. This suggests that all investigated monolayers are energetically favorable. The greater the distance between the atoms, the weaker the bond between them. Ga_2SSe is found to be the most energetically favorable with $E_{coh} = -4.01$ eV per atom. The obtained results for the cohesive energies of Ga_2XY are comparable with those of their pristine structures, such as C_{2h}-GaS 4.11 eV per atom and C_{2h}-GaSe 3.75 eV per atom,[29] and C_{3v}-Ga_2XY Janus structures, such as C_{3v}-Ga_2SSe 3.40 eV per atom and C_{3v}-Ga_2STe 3.17 eV per atom.[43]

Table 1 Lattice constants a and b, thickness Δh, anisotropic ratio $\tau = a/b$, cohesive energy E_{coh}, elastic constants C_{ij} of Janus Ga_2XY monolayers

	a (Å)	b (Å)	Δh (Å)	τ	E_{coh} (eV per atom)	C_{11} (N m^{-1})	C_{12} (N m^{-1})	C_{22} (N m^{-1})	C_{66} (N m^{-1})
Ga_2SSe	9.77	3.70	3.12	2.64	−4.01	40.50	2.58	47.47	9.24
Ga_2STe	9.82	3.87	3.30	2.54	−3.79	32.76	3.01	43.40	6.83
Ga_2SeTe	9.90	3.94	3.43	2.51	−3.63	29.01	2.56	43.05	5.64

To determine the realization of Ga_2XY monolayers, we evaluate their dynamical stability of the studied monolayers based on the calculations for phonon spectra as shown in Fig. 2(a). It is found that the phonon spectrum of Ga_2XY have 24 phonon modes due to its unit cell containing eight atoms, including three acoustic and 21 optical modes. Our calculated results indicate that there are no soft modes (negative frequencies) available in the phonon spectra of all three examined monolayers. This implies that Ga_2XY materials are dynamically stable. Further, we also test the thermodynamical stability at room temperature. The AIMD calculations are carried out at 300 K with 5 ps in increments of 1 fs. The variation of the total energy to time for these Janus monolayers is depicted in Fig. 2(b). We found that the fluctuations in the total energy of three proposed Janus structures are small during the AIMD calculations, about 0.5 eV. The crystal structure of the monolayers remains stable. No chemical bond breaks nor structural transition was observed. This proves the thermodynamical stability of the Janus Ga_2XY.

Besides the thermodynamic stability, we also test the mechanical stability of these new systems through the evaluation of their elastic constants. According to Voigt's notation, we can use four elastic constants C_{11}, C_{22}, C_{12}, and C_{66} to evaluate the mechanical stability of 2D materials. To determine these elastic constants, we apply the small tension and compression along the two x and y directions. The strain strength varies from −0.015 to 0.015 with a strain step of 0.005. At each strain value, the atomic positions are optimized and the corresponding energy data is obtained. We fit these energy values to a polynomial, thereby attaining the elastic constants C_{ij}.[44] Table 2 outlines all the values of the elastic constants of our proposed Janus systems. It is noteworthy that the elastic constants satisfy Born-Huang's criteria for mechanical stability, *i.e.* $C_{11} > 0$ and $C_{11}^2 - C_{12}^2 > 0$,[45] revealing that the Janus Ga_2XY are found to be mechanically stable.

Table 2 Bandgap E_g calculated by PBE and HSE06 methods, vacuum level difference $\Delta\Phi$, and work functions Φ of Ga_2XY monolayers

	E_g^{PBE} (eV)	E_g^{HSE06} (eV)	$\Delta\Phi$ (eV)	Φ_1 (eV)	Φ_2 (eV)
Ga_2SSe	1.88	2.67	0.15	5.34	5.49
Ga_2STe	1.41	2.15	0.38	5.44	5.06
Ga_2SeTe	1.27	1.96	0.23	5.21	4.98

The mechanical properties of materials are also characterized by Young's modulus Y_{2D} and Poisson's ratio $\mathcal{P}$. Young's modulus gives the in-plane strength of a material. Due to the anisotropic crystal structure, Young's modulus of Ga_2XY depends on the investigated direction as follows[46,47]

$$Y_{2D}(\theta) = \frac{C_{11}C_{22} - C_{12}^2}{C_{11}\sin^4\theta + C_{22}\cos^4\theta - (2C_{12} - \Omega)\sin^2\theta\cos^2\theta}, \quad (2)$$

Here $\Omega = (C_{11}C_{22} - C_{12}^2)/C_{66}$ and θ is the angle relative to the armchair axis.

Our calculated results present that Young's modulus is high directionally anisotropic due to the in-plane anisotropic lattice of Ga_2XY systems. The calculated results for Young's modulus, as shown in Fig. 3(a), indicate that Ga_2XY materials are the hardest along the [010] direction ($\theta = 90°$) with Young's modulus of Ga_2SSe, Ga_2STe, and Ga_2SeTe being 47.31, 43.12, and 42.82 N m^{-1}, respectively. Young's modulus along the [100] direction ($\theta = 0°$) is also high while the minimum value is corresponding to θ about 45° and 135°. Fig. 3 reveals that the Ga_2SSe has the largest Young's modulus in comparison with

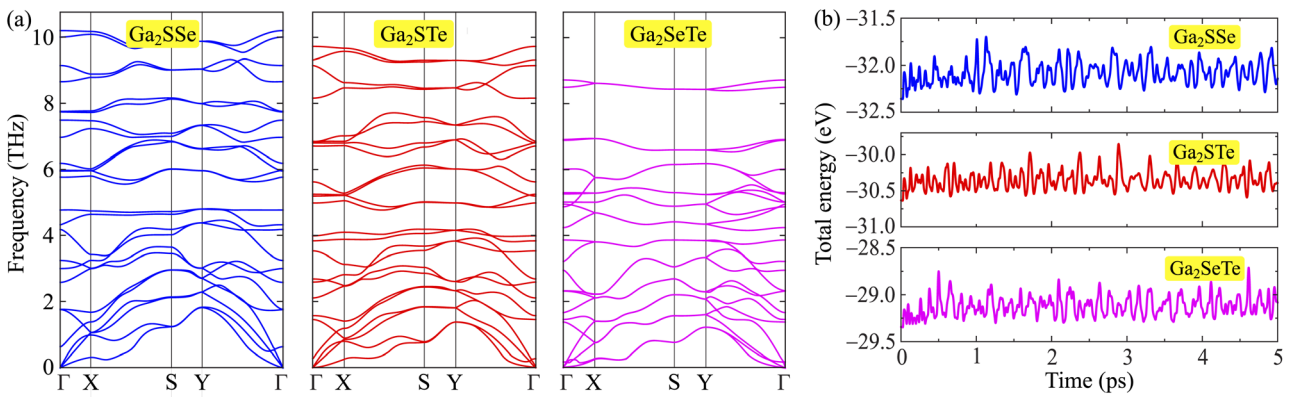

Fig. 2 (a) Phonon spectra and (b) AIMD calculation for the variations of the total energy to time of Janus Ga_2XY at room temperature.

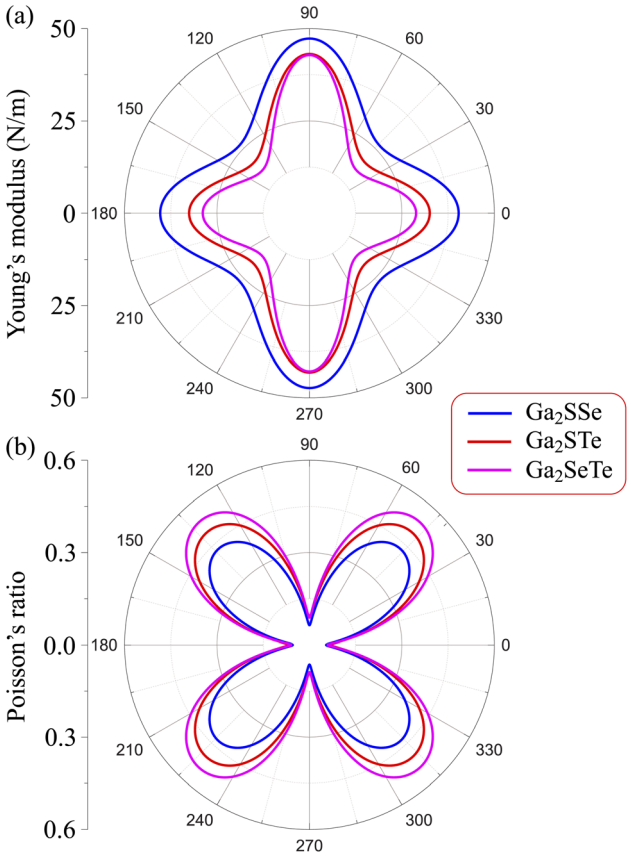

Fig. 3 Young's modulus (a) and Poisson's ratio (b) of Ga_2XY (X/Y = S, Se, Te).

other structures. The calculated values of Young's modulus decrease with increasing atomic number of chalcogen elements. This is consistent with the fact that the larger the lattice constant, the weaker the in-plane strength. In general, Ga_2XY materials are more mechanically flexible than other compounds because they have a small Young's coefficient.[48]

We also calculate Poisson's ratio $\mathcal{P}$ which can determine the mechanical response of the Ga_2XY to the applied strain as:[46,47]

$$\mathcal{P}(\theta) = \frac{C_{12}(\sin^4\theta + \cos^4\theta) - (C_{11} + C_{22} - \Omega)\sin^2\theta\cos^2\theta}{C_{11}\sin^4\theta + C_{22}\cos^4\theta - (2C_{12} - \Omega)\sin^2\theta\cos^2\theta}, \quad (3)$$

From Fig. 3(b), it is revealed that the Poisson's ratio of Ga_2XY is anisotropic, which is consistent with their in-plane anisotropic lattice. The Janus Ga_2SSe has the smallest $\mathcal{P}$ value compared with other considered structures. Thus, Poisson's ratio exhibits an opposite trend with respect to Young's modulus. It can be found that the $\mathcal{P}$ value of Ga_2XY is much smaller than that of graphene and silicene.[48] In other words, the investigated Janus monolayers are very insensitive to applied strain.

3.2 Electronic properties

In this section, we focus on the electronic properties of Janus Ga_2XY based on the DFT analysis. First, we study the band

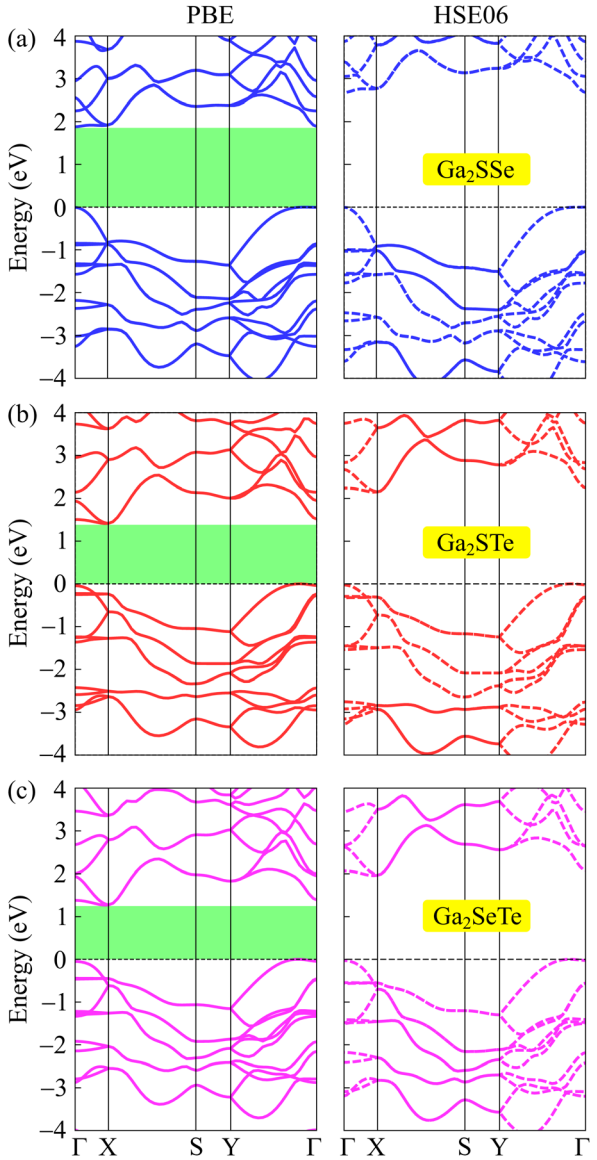

Fig. 4 Examined energy band diagrams of (a) Ga_2SSe, (b) Ga_2STe, and (a) Ga_2SeTe monolayers using the PBE and HSE06 functionals.

structures of these Janus structures using both PBE and HSE06 functionals. Fig. 4 reveals that all examined Janus materials are semiconductors. At the PBE level, the calculated bandgaps of Ga_2SSe, Ga_2STe, and Ga_2SeTe are found to be 1.88, 1.41, and 1.27 eV, respectively. It is found that all three investigated structures exhibit indirect semiconducting characteristics. However, while both Ga_2STe and Ga_2SeTe monolayer have the conduction band minimum (CBM) located at the X point and the valence band maximum located on the $Y\Gamma$ path, the CBM of Ga_2SSe located at the Γ point. However, it is worth noting that the difference in energy at the CBM and X point in Ga_2SSe is very small. These characteristics of Janus Ga_2XY in this phase are different from those in the C_{3v} one, where both C_{3v}-Ga_2STe and C_{3v}-Ga_2SeTe possess direct band gaps.[17,19] It is evident that the variation in the crystal lattice has given rise to new electronic features.

To correct the bandgaps of Ga_2XY monolayers, we also calculate the band diagrams by using the hybrid functional HSE06 as depicted in Fig. 4(b). The hybrid functional is considered to be the most efficient method to obtain the precise bandgap of semiconductors and insulators. It can be observed that all Janus monolayers retain the bandgap nature at the PBE level. However, the bandgaps calculated by the HSE06 method is much higher than those by the PBE method as tabulated in Table 2. At the HSE06 level, the bandgaps of Ga_2XY semiconductors vary from 1.96 to 2.67 eV. The bandgaps of these structures are comparable with that of C_{3v}-Ga_2XY structures.[16]

To further understand the nature of the electronic structure, we explore the weighted bands of Janus Ga_2XY as revealed in Fig. 5. It is obvious that all three Janus Ga_2XY monolayers exhibit the same trend in the contributions of the atomic orbitals to the electronic bands. The main component of the conduction band is the s orbital of the Ga atom, while the major contribution of the valence band is the p orbital of the chalcogen atom.

One of the important features of electronic materials is the work function, which represents the ability of electrons to escape from the surface of a material. Possessing the vertical asymmetric lattice, Janus structures possess intrinsic electric fields.[49] The magnitude of this electric field depends on the electronegativity difference of the X and Y sides. For the asymmetric structures, we included the dipole correction[50] in the calculations of the electrostatic potentials. Fig. 6 depicts the computed the electrostatic potential with dipole correction. We

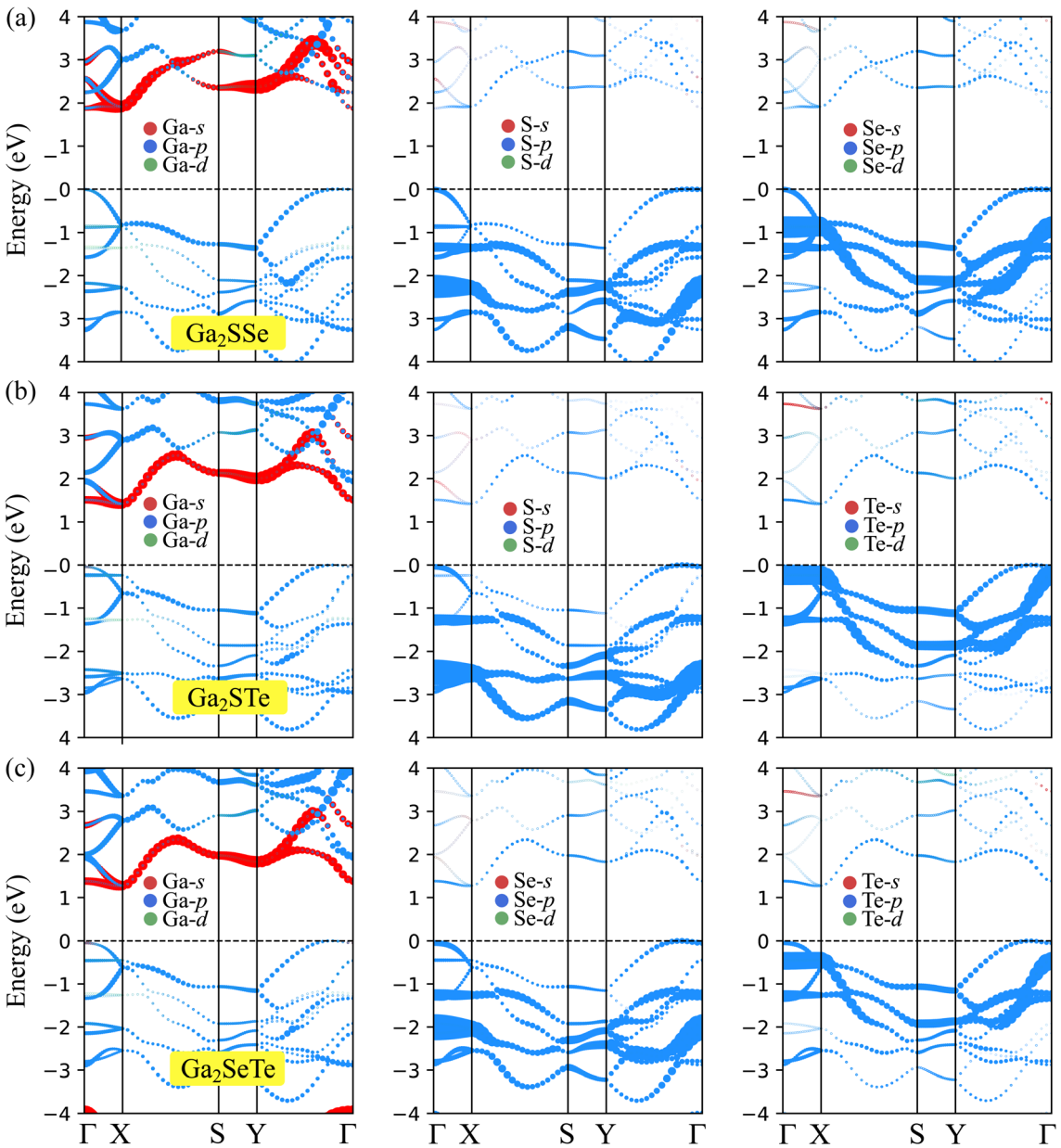

Fig. 5 Projected band structures of (a) Ga_2SSe, (b) Ga_2STe, and (a) Ga_2SeTe.

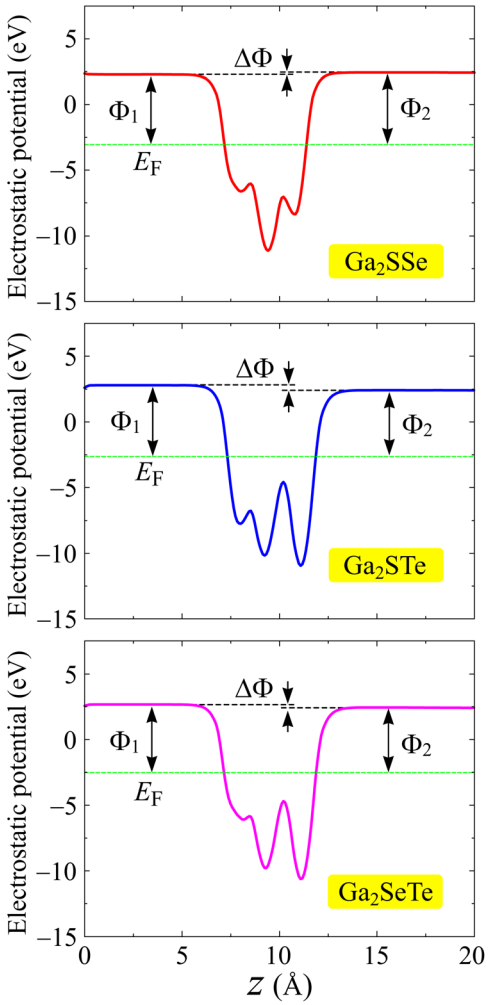

Fig. 6 Calculated electrostatic potentials with dipole corrections of Ga_2XY monolayers.

can see that a distinct vacuum level difference $\Delta\Phi$ is found at the surfaces of Janus Ga_2XY. The larger the atomic size difference between X and Y constituent elements, the higher value of $\Delta\Phi$ is. From Table 2, we can see that, for example, the values of $\Delta\Phi$ for Ga_2SSe and Ga_2STe are 0.15 and 0.38 eV, respectively. The value of $\Delta\Phi$ not only affects the work functions on the surfaces of the materials but also affects the photocatalytic performances of the 2D materials. The value of the work function is determined based on the difference between the Fermi level and the vacuum level. The X and Y surfaces of Janus have different vacuum levels, leading to a disparity in the work functions at the two surfaces. The obtained work functions on both surfaces of Ga_2XY are summarized in Table 2. It is demonstrated that the values of the work function on the X side are in the range from 5.21 to 5.44 eV, while those on the Y side are in the range from 4.98 to 5.49 eV. Furthermore, Janus Ga_2SeTe has the smallest work function at the two surfaces compared with the other Ga_2XY structures. This means that it is easier for the electron escaping from the surfaces of Ga_2SeTe compound than for the other structures.

3.3 Carrier mobilities

Mobility of carriers is one of the key parameters affecting the applicability of the material to electronics and optoelectronics. We here examine the carrier mobility of three studied Janus compounds through the deformation potential (DP) theory suggested by Bardeen and Shockley.[41] The carrier mobility of a 2D crystal is defined as follows:

$$\mu_{2D} = \frac{e\hbar^3 C_{2D}}{k_B T m^* \bar{m} E_d^2}, \quad (4)$$

where e stands for the elementary charge, $\hbar$ refers to the reduced Planck's constant, k_B is Boltzmann's constant, m^* is the carrier effective mass, and $\bar{m}$ denotes the average effective mass

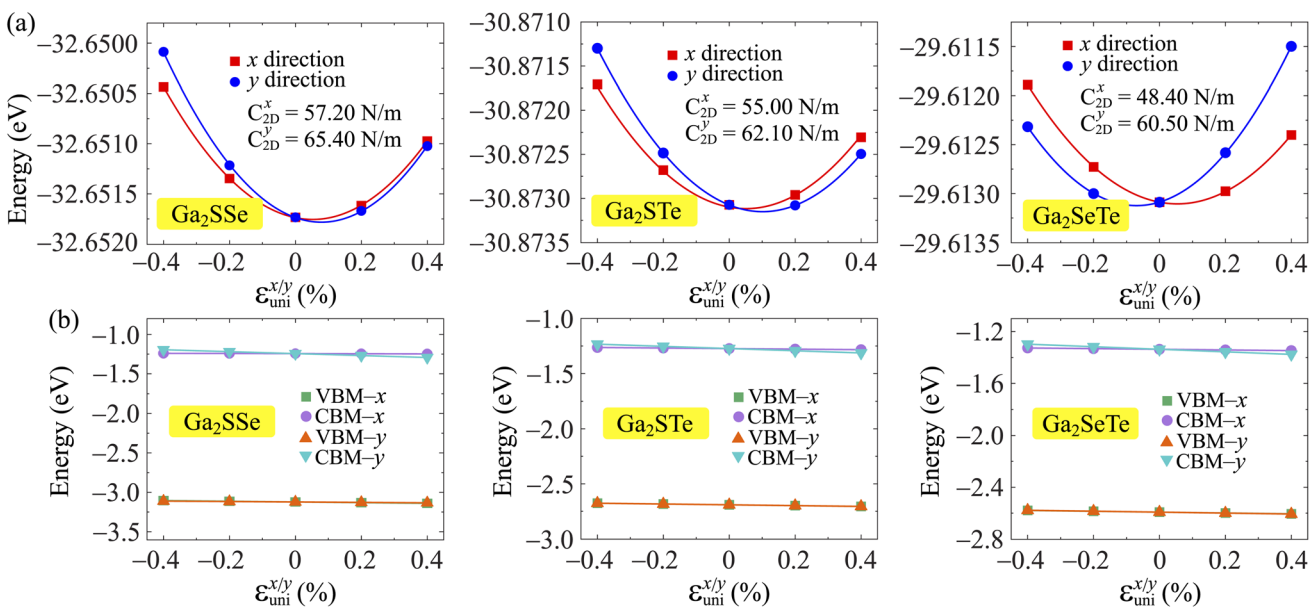

Fig. 7 Uniaxial strain-dependence of the total energies (a) and band-edge energies (b) of Ga_2XY. The data fitting is represented by the solid line.

Table 3 The carrier effective mass m^* (in unit of the free electron mass m_0), elastic modulus C_{2D} (Nm^{-1}), DP constant E_d (eV), and mobility of carriers μ ($cm^2\ V^{-1}\ s^{-1}$) along the x/y direction of Janus Ga_2XY

		m_x^*	m_y^*	${C_{2D}}^x$	${C_{2D}}^y$	${E_{2D}}^x$	${C_{2D}}^y$	μ_x	μ_y
Ga_2SSe	Electron	0.99	0.24	57.20	65.40	−0.89	−12.31	3.22×10^3	78.47
	Hole	8.60	1.80	57.20	65.40	−4.34	−2.74	1.91	26.26
Ga_2STe	Electron	0.86	0.23	55.00	62.10	−2.52	−10.01	485.69	130.57
	Hole	2.35	1.26	55.00	62.10	−3.67	−3.64	21.48	45.98
Ga_2SeTe	Electron	0.68	0.39	48.40	60.5	−2.54	−9.88	459.09	66.01
	Hole	1.56	1.06	48.40	60.5	−3.34	−3.63	46.09	71.89

($\overline{m} = \sqrt{m_x m_y}$). T is the temperature set to be 300 K, E_d is the DP constant, and C_{2D} is the elastic modulus. The DP constant derives from $E_d = \frac{\Delta E_{edge}}{\varepsilon_{uni}}$, where ΔE_{edge} is the displacement of the CBM (for electrons) and VBM (for holes) caused by the uniaxial strain ε_{uni}. The displacement of these band edges is determined with respect to the vacuum level. By linearly fitting the energy shift of the CBM and VBM as a function of the uniaxial strains as shown in Fig. 7, we obtain the DP constant. The elastic modulus C_{2D} is determined by $C_{2D} = \frac{1}{S}\frac{\partial^2 E}{\partial {\varepsilon_{uni}}^2}$, where E is the total energy of the system, S is the area of the supercell at equilibrium. The carrier effective mass is determined by $\frac{1}{m^*} = \frac{1}{\hbar^2}\left|\frac{\partial^2 E(k)}{\partial k^2}\right|$. The effective masses of carriers can be calculated by the parabolic fitting of the values of energies around the CBM and VBM.

Table 3 reports the data of the carrier effective mass, elastic modulus, and DP constant of Ga_2XY monolayers along the x and y directions. Based on these obtained parameters, the carrier mobilities in all of Janus are attained accordingly. It is found that the electron and hole mobilities are different in the x and y transport directions, indicating that the carrier mobilities are directionally anisotropic. Particularly, the carrier mobility of Ga_2SSe exhibits high anisotropic, where the mobility of electrons along the x direction is much higher than that along the y direction. Ga_2SSe monolayer possesses high electron mobility along the x direction up to $\mu_x = 3.22 \times 10^3\ cm^2\ V^{-1}\ s^{-1}$. Similarly, the μ_x values of Ga_2STe and Ga_2SeTe are found respectively to be 485.69 and 459.09 $cm^2\ V^{-1}\ s^{-1}$, which are much higher than their electron mobilities along the y direction μ_y as presented in Table 3. The carrier mobilities of Ga_2STe and Ga_2SeTe are comparable to those of the C_{2h}-GaS, C_{2h}-GaSe while Janus Ga_2SSe monolayer possesses superior electron mobility compared to that of the pristine C_{2h}-GaX structures.[29] However, the electron carrier of Janus Ga_2SSe is one order of magnitude smaller than that of the Janus C_{3v}-Ga_2SSe ($1.31 \times 10^4\ cm^2\ V^{-1}\ s^{-1}$).[51]

4 Conclusion

The structural stability, electronic characteristics, and carrier mobilities of Janus materials based on the C_{2h} phase of group III monochalcogenide Ga_2XY were investigated using first-principles calculations. Through AIDM calculations and Born-Huang's criteria, all three Janus Ga_2XY monolayers are confirmed to be structural stability. The obtained results indicated that Ga_2XY monolayers exhibit anisotropic mechanical properties and Ga_2XY monolayers are more mechanically flexible than graphene and silicene. Ga_2XY monolayers were found to be semiconductors with indirect bandgaps from 1.96 to 2.67 eV at the HSE06 level. With the vertical asymmetric lattice, the distinct vacuum level difference $\Delta\Phi$ was observed at the surfaces of Janus Ga_2XY and the values of $\Delta\Phi$ depend highly on the atomic size of the constituent atoms X and Y. The obtained results demonstrated that Ga_2XY materials exhibit high directional anisotropy. Particularly, the electron mobility of Ga_2SSe was found up to $3.22 \times 10^3\ cm^2\ V^{-1}\ s^{-1}$, which is potential for applications in nanoelectronic devices.

Conflicts of interest

There are no conflicts of interest to declare.

Acknowledgements

This work belongs to the project grant No: T2022-23 funded by Ho Chi Minh City University of Technology and Education (Vietnam).

References

1 W. Feng, X. Zhou, W. Q. Tian, W. Zheng and P. Hu, *Phys. Chem. Chem. Phys.*, 2015, **17**, 3653.
2 A. Harvey, C. Backes, Z. Gholamvand, D. Hanlon, D. McAteer, H. C. Nerl, E. McGuire, A. Seral-Ascaso, Q. M. Ramasse, N. McEvoy, S. Winters, N. C. Berner, D. McCloskey, J. F. Donegan, G. S. Duesberg, V. Nicolosi and J. N. Coleman, *Chem. Mater.*, 2015, **27**, 3483.
3 P. Hu, Z. Wen, L. Wang, P. Tan and K. Xiao, *ACS Nano*, 2012, **6**, 5988.
4 S. Demirci, N. Avazli, E. Durgun and S. Cahangirov, *Phys. Rev. B*, 2017, **95**, 115409.
5 V. T. Vi, N. N. Hieu, B. D. Hoi, N. T. Binh and T. V. Vu, *Superlattices Microstruct.*, 2020, **140**, 106435.
6 A. V. Lugovskoi, M. I. Katsnelson and A. N. Rudenko, *Phys. Rev. Lett.*, 2019, **123**, 176401.
7 A.-Y. Lu, H. Zhu, J. Xiao, C.-P. Chuu, Y. Han, M.-H. Chiu, C.-C. Cheng, C.-W. Yang, K.-H. Wei, Y. Yang, Y. Wang, D. Sokaras, D. Nordlund, P. Yang, D. A. Muller,

M.-Y. Chou, X. Zhang and L.-J. Li, *Nat. Nanotechnol.*, 2017, **12**, 744.
8 J. Zhang, S. Jia, I. Kholmanov, L. Dong, D. Er, W. Chen, H. Guo, Z. Jin, V. B. Shenoy, L. Shi and J. Lou, *ACS Nano*, 2017, **11**, 8192–8198.
9 T. V. Vu, V. T. T. Vi, H. V. Phuc, A. I. Kartamyshev and N. N. Hieu, *Phys. Rev. B*, 2021, **104**, 115410.
10 F. Li, W. Wei, P. Zhao, B. Huang and Y. Dai, *J. Phys. Chem. Lett.*, 2017, **8**, 5959–5965.
11 L. Dong, J. Lou and V. B. Shenoy, *ACS Nano*, 2017, **11**, 8242–8248.
12 A. Mogulkoc, Y. Mogulkoc, S. Jahangirov and E. Durgun, *J. Phys. Chem. C*, 2019, **123**, 29922–29931.
13 N. N. Hieu, H. V. Phuc, A. I. Kartamyshev and T. V. Vu, *Phys. Rev. B*, 2022, **105**, 075402.
14 T. V. Vu, C. V. Nguyen, H. V. Phuc, A. A. Lavrentyev, O. Y. Khyzhun, N. V. Hieu, M. M. Obeid, D. P. Rai, H. D. Tong and N. N. Hieu, *Phys. Rev. B*, 2021, **103**, 085422.
15 H. T. T. Nguyen, V. T. T. Vi, T. V. Vu, N. V. Hieu, D. V. Lu, D. P. Rai and N. T. T. Binh, *RSC Adv.*, 2020, **10**, 44785–44792.
16 A. Huang, W. Shi and Z. Wang, *J. Phys. Chem. C*, 2019, **123**, 11388.
17 T. V. Vu, V. T. T. Vi, C. V. Nguyen, H. V. Phuc and N. N. Hieu, *J. Phys. D: Appl. Phys.*, 2020, **53**, 455302.
18 T. V. Vu, V. T. T. Vi, H. V. Phuc, C. V. Nguyen, N. A. Poklonski, C. A. Duque, D. P. Rai, B. D. Hoi and N. N. Hieu, *J. Phys.: Condens. Matter*, 2021, **33**, 225503.
19 H. T. Nguyen, V. T. Vi, T. V. Vu, H. V. Phuc, C. V. Nguyen, H. D. Tong, L. T. Hoa and N. N. Hieu, *Phys. E*, 2020, **124**, 114358.
20 M. Demirtas, B. Ozdemir, Y. Mogulkoc and E. Durgun, *Phys. Rev. B*, 2020, **101**, 075423.
21 J. L. Zhang, S. Zhao, C. Han, Z. Wang, S. Zhong, S. Sun, R. Guo, X. Zhou, C. D. Gu, K. D. Yuan, Z. Li and W. Chen, *Nano Lett.*, 2016, **16**, 4903–4908.
22 S. Y. Lim, J.-U. Lee, J. H. Kim, L. Liang, X. Kong, T. T. H. Nguyen, Z. Lee, S. Cho and H. Cheong, *Nanoscale*, 2020, **12**, 8563–8573.
23 S. Shi, Z. Sun and Y. H. Hu, *J. Mater. Chem. A*, 2018, **6**, 23932–23977.
24 X. Li and H. Zhu, *J. Materiomics*, 2015, **1**, 33–44.
25 Y. Sun, Y. Li, T. Li, K. Biswas, A. Patanè and L. Zhang, *Adv. Funct. Mater.*, 2020, **30**, 2001920.
26 D. A. Bandurin, A. V. Tyurnina, G. L. Yu, A. Mishchenko, V. Zólyomi, S. V. Morozov, R. K. Kumar, R. V. Gorbachev, Z. R. Kudrynskyi, S. Pezzini, Z. D. Kovalyuk, U. Zeitler, K. S. Novoselov, A. Patanè, L. Eaves, I. V. Grigorieva, V. I. Fal'ko, A. K. Geim and Y. Cao, *Nat. Nanotechnol.*, 2017, **12**, 223–227.
27 D. Errandonea, D. Martínez-García, A. Segura, A. Chevy, G. Tobias, E. Canadell and P. Ordejon, *Phys. Rev. B: Condens. Matter Mater. Phys.*, 2006, **73**, 235202.
28 L. Ghalouci, F. Taibi, F. Ghalouci and M. Bensaid, *Comput. Mater. Sci.*, 2016, **124**, 62–77.
29 T. Hu, C. Xu, A. Zhang and P. Yu, *Mater. Adv.*, 2022, **3**, 2213–2221.
30 P. Giannozzi, S. Baroni, N. Bonini, M. Calandra, R. Car, C. Cavazzoni, D. Ceresoli, G. L. Chiarotti, M. Cococcioni, I. Dabo, A. D. Corso, S. de Gironcoli, S. Fabris, G. Fratesi, R. Gebauer, U. Gerstmann, C. Gougoussis, A. Kokalj, M. Lazzeri, L. Martin-Samos, N. Marzari, F. Mauri, R. Mazzarello, S. Paolini, A. Pasquarello, L. Paulatto, C. Sbraccia, S. Scandolo, G. Sclauzero, A. P. Seitsonen, A. Smogunov, P. Umari and R. M. Wentzcovitch, *J. Phys.: Condens. Matter*, 2009, **21**, 395502.
31 P. E. Blöchl, *Phys. Rev. B: Condens. Matter Mater. Phys.*, 1994, **50**, 17953.
32 J. P. Perdew, K. Burke and M. Ernzerhof, *Phys. Rev. Lett.*, 1996, **77**, 3865.
33 J. Heyd, G. E. Scuseria and M. Ernzerhof, *J. Chem. Phys.*, 2003, **118**, 8207.
34 G. Kresse and J. Furthmüller, *Phys. Rev. B: Condens. Matter Mater. Phys.*, 1996, **54**, 11169–11186.
35 G. Kresse and J. Furthmüller, *Comput. Mater. Sci.*, 1996, **6**, 15–50.
36 J. D. Pack and H. J. Monkhorst, *Phys. Rev. B: Solid State*, 1977, **16**, 1748–1749.
37 S. Grimme, J. Antony, S. Ehrlich and H. Krieg, *J. Chem. Phys.*, 2010, **132**, 154104.
38 T. Sohier, M. Calandra and F. Mauri, *Phys. Rev. B*, 2017, **96**, 075448.
39 A. Togo, L. Chaput and I. Tanaka, *Phys. Rev. B: Condens. Matter Mater. Phys.*, 2015, **91**, 094306.
40 S. Nosé, *J. Chem. Phys.*, 1984, **81**, 511.
41 J. Bardeen and W. Shockley, *Phys. Rev.*, 1950, **80**, 72.
42 T. V. Vu, V. T. T. Vi, C. V. Nguyen, H. V. Phuc and N. N. Hieu, *J. Phys. D: Appl. Phys.*, 2020, **53**, 455302.
43 Y. Bai, Q. Zhang, N. Xu, K. Deng and E. Kan, *Appl. Surf. Sci.*, 2019, **478**, 522–531.
44 K.-A. N. Duerloo, M. T. Ong and E. J. Reed, *J. Phys. Chem. Lett.*, 2012, **3**, 2871–2876.
45 M. Born and K. Huang, *Am. J. Phys.*, 1955, **23**, 474.
46 N. T. Hung, A. R. T. Nugraha and R. Saito, *J. Phys. D: Appl. Phys.*, 2018, **51**, 075306.
47 P. Xiang, S. Sharma, Z. M. Wang, J. Wu and U. Schwingenschlögl, *ACS Appl. Mater. Interfaces*, 2020, **12**, 30731.
48 H. Şahin, S. Cahangirov, M. Topsakal, E. Bekaroglu, E. Akturk, R. T. Senger and S. Ciraci, *Phys. Rev. B: Condens. Matter Mater. Phys.*, 2009, **80**, 155453.
49 C.-F. Fu, J. Sun, Q. Luo, X. Li, W. Hu and J. Yang, *Nano Lett.*, 2018, **18**, 6312–6317.
50 L. Bengtsson, *Phys. Rev. B: Condens. Matter Mater. Phys.*, 1999, **59**, 12301.
51 B. Sa, X. Shen, S. Cai, Z. Cui, R. Xiong, C. Xu, C. Wen and B. Wu, *Phys. Chem. Chem. Phys.*, 2022, **24**, 15376–15388.